Received: 5 June 2021 | Revised: 12 August 2021 | Accepted: 5 September 2021

DOI: 10.1002/app.51664

ARTICLE

Applied Polymer SCIENCE WILEY

Rheology, dispersion, and cure kinetics of epoxy filled with amine- and non-functionalized reduced graphene oxide for composite manufacturing

Annika C. Ackermann[1,2,3] | **Stefan Carosella**[1,3] | **Markus Rettenmayr**[4] | **Bronwyn L. Fox**[2,3] | **Peter Middendorf**[1,3]

[1]Institute of Aircraft Design, University of Stuttgart, Stuttgart, Germany

[2]Faculty of Science, Engineering and Technology, Swinburne University of Technology, Melbourne, Victoria, Australia

[3]ARENA2036 Research Campus, Stuttgart, Germany

[4]Department of Metallic Materials, Otto Schott Institute of Materials Research, Friedrich-Schiller-University Jena, Jena, Germany

Correspondence
Annika C. Ackermann, Institute of Aircraft Design, University of Stuttgart, Pfaffenwaldring 31, 70569, Stuttgart, Germany.
Email: ackermann@ifb.uni-stuttgart.de

Funding information
Bundesministerium für Bildung und Forschung, Grant/Award Number: 02P18Q643; Deutsche Forschungsgemeinschaft, Grant/Award Number: DFG Inst275/391-1

Abstract

This study evaluates the effect of plasma surface functionalization of reduced graphene oxide particles on the processing characteristics and homogeneity of dispersion of a bisphenol A-(epichlorhydrin) epoxy matrix and amine-based hardener with varying weight fractions from 0.00 to 1.50 wt%. It was observed that amine-functionalized reduced graphene oxide leads to a more drastic viscosity increase of up to 18-fold of the uncured suspensions and that its presence influences the conversion rates of the curing reaction. Optical microscopy of thin sections and transmission electron microscopy analysis showed that a more homogeneous dispersion of the particles could be achieved especially at higher weight fractions by using an appropriate surface functionalization. This knowledge can be used to define suitable processing conditions for epoxies with amine-based hardeners depending on the loading and functionalization of graphene-related particles.

1 | INTRODUCTION

Increasing demands on the thermal, mechanical, and electrical properties of composite materials require the incorporation of new materials such as graphene and its related materials. Due to the particular arrangement of its carbon atoms, graphene as well as its derivatives demonstrate outstanding mechanical, thermal, and electrical properties[1–3] whilst having a very large surface area.[4] This allows a significant change of the material properties of composite materials at very low nanoparticle loadings.[5]

However, the integration of graphene-related materials into polymers poses a number of challenges as the particles tend to be chemically inert and form agglomerates that can later act as failure points in the composite.[6,7] Furthermore, the available process windows during manufacturing are reduced as the viscosity of the suspensions is increased significantly by the presence of graphene-related materials.[8,9] A number of researchers

try to overcome these issues by the use of different solvents such as acetone,[10] isopropanol,[11,12] or N-methyl-2-pyrrolidone,[13] but these come at the cost of environmental issues, additional time-intensive processing steps and residual impurities that can influence the cross-linking process and, hence, alter the properties of the matrix significantly.[14–16] In contrast to this, a tailored functionalization of the surface of graphene-related particles can add functional groups and activate the carbon surface to facilitate a homogeneous dispersion of the particles in the polymer whilst improving the interfacial bonds between the particle and the polymer.[17–20] A well-dispersed suspension should therefore be regarded as a goal in the production of nanocomposites, but the strong interfacial bonding is also associated with a higher viscosity of the suspension[21] and may also modify the curing reaction.[22,23]

It is possible to distinguish between two different approaches to functionalize carbon-based nanomaterials: covalent and non-covalent functionalization. Non-covalent functionalization processes do not change the chemical or electronic structure of the particle, but call for a complicated chemical synthesis including a time-consuming cleaning process of the particles. The hereby-created functional groups are easy to remove as they are dependent on weak attractive forces such as hydrogen bonding, van der Waals forces, π–π stacking, hydrophobic or ionic interactions.[24–26] In contrast to this, a covalent functionalization, such as chemical or plasma modification, enables a much larger range of different properties, but can transform the structure of the carbon material as the functional groups are bonded to the carbon lattice via altering the carbon structure.[24] Chemical functionalization usually relies on the use of large volumes of organic or hazardous solvents and reagents that are harmful to the environment, require a large number of different, non-robust and time-consuming processing steps with constrained scalability and time-intensive purification.[27,28] Plasma treatment does not require the extensive amount of chemicals as its working principle relies on the use of the ionized forms of gases such as O_2, NH_3 or CF_4 that must be applied with specialized equipment with explosion protection devices.[24] During the functionalization process, the excited gas species destroys the covalent bonds on the material surface up to depths of a few nanometers.[29] In the case of single-layer graphene, this implies that the material would be affected in its entire structure. On the contrary, few-layer graphene as well as multilayer reduced graphene oxide would experience changes to its exposed surfaces (i.e. the outer layers and the edges of graphene sheets), but the inner graphene layers remain unchanged. The activated surface of the particle can now react with the plasma to create functional groups without leading to major modifications of the composition of the bulk material.[30,31] It is a quick process with typical processing times of seconds to a few minutes without subsequent purification of the treated material.[32] Given that the functional groups are etched and grafted onto the surface of the particles, the surface roughness is increased.[33] Furthermore, the creation of defects and functional groups on the surface of the particle may lead to an inferior electrical conductivity.[34,35]

An amine surface functionalization is of particular importance in the case of epoxies as these functional groups can act as a cross-linker to form covalent bonds with epoxy or as a modifier in the nanocomposite structure. The amine groups can undergo a chemical reaction with epoxy resins via an amide bond that leads to a better dispersion of the particles, an enhanced interfacial adhesion as well as load transfer that may enhance the mechanical and thermal properties of the composite material.[17,21,23,36]

The impact of the plasma functionalization process on the quality of graphene and its derivatives has, however, not been investigated intensively. Furthermore, the influence of the functionalization on the processing behavior and the quality of the composite remains uncertain. This study reports the findings of a number of tests with varying reduced graphene oxide contents in a bisphenol A-(epichlorhydrin) epoxy matrix with an amine-based hardener and different types of chemical functionalization, which was achieved using plasma treatment of the nanoparticles. Reduced graphene oxide was chosen as the type of graphene derivative since it is readily available in large volumes and at comparatively low costs which allows the mass-production of composite materials with graphene-related materials.[37] First, the impact of the plasma processing on the quality of the used amine-functionalized form of reduced graphene oxide (frGO) was compared to the non-functionalized form of reduced graphene oxide (rGO). Second, the processability of the rGO- and frGO-including epoxy/hardener suspensions was assessed for loadings from 0.00 to 1.50 wt% with respect to viscosity, degree of dispersion, and curing behavior. This information can be applied to predict the impact of amine-functionalized graphene derivatives in comparison to non-functionalized graphene derivatives on the manufacturing processes of composite materials using bisphenol A-(epichlorhydrin) epoxy resins with amine-based hardeners as the matrix material. The use of such a tailored surface functionalization will allow improved material properties such as the Young's modulus,[7,38] electrical[39,40] or thermal conductivity[40,41] of the resulting composite. It will also offer further areas of applications such as electromagnetic shielding[42] or strain

monitoring by using the piezoelectric properties of graphene and its derivatives[43].

2 | MATERIALS AND METHODS

2.1 | Materials

Two varieties of graphene-related materials in the form of non-functionalized reduced graphene oxide EXG 98300 R (rGO) and amine-functionalized reduced graphene oxide EXG 98300 R FNH (frGO) were provided by Graphit Kropfmühl GmbH. Both materials were produced by the manufacturer using a modified Hummers' method and subsequently reduced by thermal treatment using 500 µm graphite flakes (RFL 99,5 O) as the starting material. The frGO powder underwent a further cold plasma process by the manufacturer with NH_3 being the source for the low-pressure gas plasma and, thus, creating an amine functionalization on the particles. The powder materials were used as received.

Sika Deutschland GmbH supplied the bisphenol A-(epichlorhydrin) epoxy resin Biresin® CR83 and the amine-based hardener Biresin® CH83-10. It is a two-part resin system with a low mixed viscosity (155 mPa s at 25°C) which further aids the dispersion of the used graphene-related particles.

2.2 | Sample preparation

The three roll mill 80S PLUS from EXAKT Advanced Technologies GmbH was used to disperse the rGO and frGO particles in the epoxy resin. It was operated at a speed ratio of 1:3:9 where the velocity of the fastest roller was set to 200 rpm. The rGO or frGO powder and resin were premixed by hand and this material was led through the three roll mill using eight cycles where the respective gap widths followed the procedure as shown in Table 1. This procedure was used to create a masterbatch that can be used to achieve a maximum concentration of 1.50 wt% of rGO or frGO in the final nanocomposite. After the dispersion process, the hardener was added and, if required, the masterbatch was diluted to lower rGO or frGO concentrations by adding more resin. The suspension was subsequently stirred by hand and degassed in a vacuum chamber. The general approach is illustrated in Figure 1.

2.3 | Characterization

Statistical Raman spectroscopy[44] was used to approximate the level of defects in the powder materials. It was executed using a WITec alpha 300M+ system with a 532 nm laser and a 50× objective lens. The powder was deposited on double-sided tape being placed on a glass slide. An area of 100 × 100 µm with a total of 1600 data points for each material was evaluated with one accumulation of 4 s each.

TABLE 1 Gap widths used for the dispersion process of the different suspensions in the three roll mill

Cycle number	Width of first gap (µm)	Width of second gap (µm)
1	90	30
2	90	30
3	60	20
4	60	20
5	30	10
6	30	10
7	15	5
8	15	5

Brunauer–Emmett–Teller (BET) theory was performed on the rGO and frGO materials to evaluate the specific surface area. The measurements were conducted using a Micromeritics TriStar 3000 and based on DIN ISO 9277:2010[45]. The mass of each sample was in the range of 0.2–0.3 g and the samples were prepared for analysis for 20 min under the influence of a vacuum at 250°C and subsequently left to cool to room temperature. Nitrogen was used as the gaseous adsorbate and the respective BET specific surface area was calculated for each material based on five measurement points.

The rheological behavior with examination of the occurring viscosities and shear stresses of the epoxy/hardener suspensions was carried out using a Physica MCR 301 stress-controlled rotational rheometer from Anton Paar. A plate-plate setup was used in which the upper plate (PP25) had a radius of 12.5 mm. The samples were transferred to the lower plate with a pipette. After the upper plate was lowered to the measuring position (gap width of 1 mm), the samples were kept at a measuring temperature of 25°C to reach equilibrium. The temperature was kept constant at 25 ± 0.01°C by the use of a Peltier element. Subsequently, the measurements were conducted for shear rates from 2 to 100 s^{-1} where the shear rate increased linearly during an interval of 140 s. Measurements for each suspension were obtained from five new portions of the respective material.

Differential scanning calorimetry (DSC) was conducted in accordance to DIN 65467:1999[46] and using a DSC 2920 from TA Instruments to determine the reaction enthalpy of the curing reaction. Each measurement took place in a nitrogen atmosphere and the respective

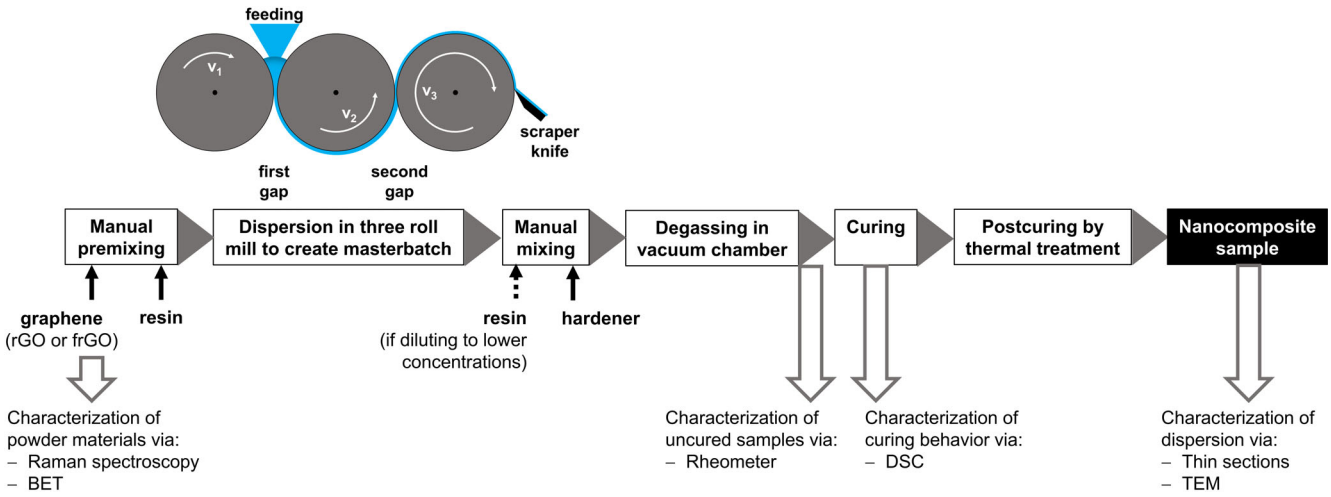

FIGURE 1 Schematic showing the general approach of sample characterization and preparation applied in this study [Color figure can be viewed at wileyonlinelibrary.com]

uncured sample was kept at −5°C for 5 min. It was then heated from −5 to 250°C at a heating rate of 10°C min^{-1}. The reaction enthalpy of the curing reaction was assessed based on five new samples of the respective material.

Thin sections of the nanocomposite samples with a thickness of 8 μm were prepared with a sliding microtome POLYCUT E from Reichert-Jung. These thin section samples were analyzed using the optical microscope SZX10 from Olympus to examine the broad dispersion of the rGO and frGO particles within the matrix.

Transmission electron microscopy (TEM) was carried out using a JEM-ARM200F from Jeol equipped with a Gatan Spektrometer (Model 977 Enfinium ER for EELS and Dual EELS) filter and operating at an accelerating voltage of 200 keV. The nanocomposite specimens for TEM observation were fabricated with a thickness of approximately 100 nm using a Leica Ultracut UCT. The sections were collected on a copper grid.

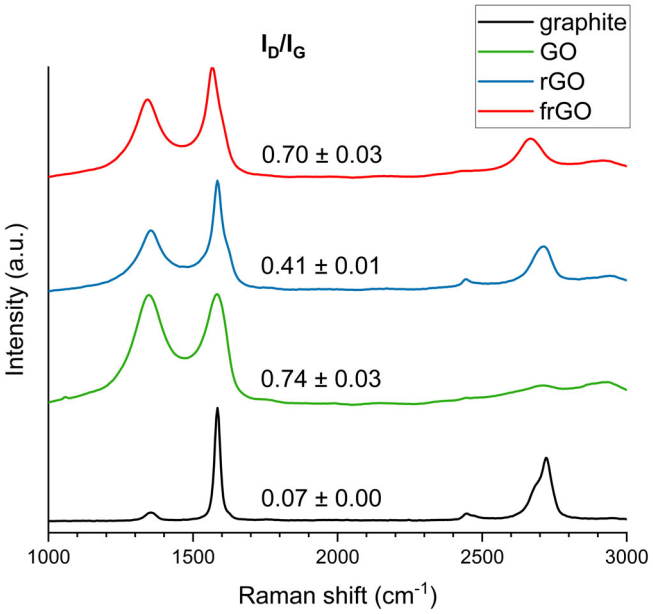

FIGURE 2 Mean Raman spectra of graphite, GO, rGO and frGO as obtained by statistical Raman spectroscopy and shifted consecutively to aid the reader. The respective I_D/I_G ratio is labeled [Color figure can be viewed at wileyonlinelibrary.com]

3 | RESULTS AND DISCUSSION

3.1 | Characterization of powder materials

The level of defects in graphene-related materials is crucial for their mechanical, thermal, and electrical properties and should be kept at a minimum. A suitable method to assess the level of disorder in graphene and its derivatives is Raman spectroscopy. The Raman spectra of the powder materials used in this work are illustrated in Figure 2. The peak intensity ratio I_D/I_G of the D-peak (~1350 cm^{-1}) and the G-peak (~1580 cm^{-1}) was used to approximate the level of disorder and, thus, the level of defects within the rGO and frGO samples[47,48]. Given that the manufacturing process of the graphene-related particles was based on a modified Hummers' method that relies on the oxidation and reduction of the particles, the level of disorder of graphite is lower than for rGO and frGO. The level of disorder of frGO as measured by the I_D/I_G ratio is significantly larger to the I_D/I_G ratio of rGO and similar to the intermediate product graphene oxide (GO) indicating more defects in the frGO material by the functionalization process by plasma processing. The peak

intensity ratio I_{2D}/I_G can give an indication of the number of layers in a graphene-related material[48]. Given that none of the particles is a single or bilayer graphene, only a small 2D-peak (~2700 cm^{-1}) was detected for all samples.

The respective BET surface area of the rGO and frGO powders are shown in Table 2. As expected, the measured surface areas were below the theoretical surface area of single layer graphene (~2600 $m^2\ g^{-1}$),[4,49] but are comparable with research carried out by Fan et al. (365 $m^2\ g^{-1}$)[50] and Wang et al. (320 $m^2\ g^{-1}$)[51]. As in our work, both works applied the modified Hummers' method to produce their graphene-related materials. In contrast to Mohan et al.,[52] who determined that the presence of functionalization led to an increase of the BET surface area, the materials used in this work show no significant effect of the present functionalization. This difference suggests that the chemical functionalization as conducted by Mohan et al. may lead to a stronger transformation of the carbon lattice with possibly some further exfoliation of the particles than the plasma treatment of the particles in this work.

TABLE 2 Mean Brunauer–Emmett–Teller (BET) surface area and respective expanded uncertainty for a coverage probability of 95% of the different powder materials

Material	BET surface area ($m^2\ g^{-1}$)
rGO	301.8 ± 5.2
frGO	308.2 ± 4.2

3.2 | Rheological behavior

The viscosity of a suspension is crucial for its processing behavior as high viscosities can lead to a challenging processability, inclusions of air and, in the case of fiber-reinforced polymers, can limit the sufficient wetting of the fibers. Figure 3a illustrates the change of shear stress over a range of shear rates for suspensions with various rGO and frGO loadings. For all samples, a growing shear stress was observed for both increasing shear rates and increasing weight fractions. This finding is also illustrated in Figure 4 that shows the change in shear stresses for three exemplary shear rates of 2, 51 and 100 s^{-1} with respect to varying contents of rGO and frGO. For both forms of graphene derivatives, an increase in the present shear stresses occurred with increasing loadings, but the effect of the presence of the used particles was more dominant in the range of 1.00 to 1.50 wt% than for loadings of 0.25 to 1.00 wt%. Furthermore, the form of graphene-related material also exhibited a different degree of impact on the present shear stress. For the range from 0.25 to 0.75 wt%, the effect on the shear stresses was more dominant in the case of rGO than in the case of frGO. On the contrary, the effect of the additive was more pronounced for frGO than for rGO in the range of 0.75 to

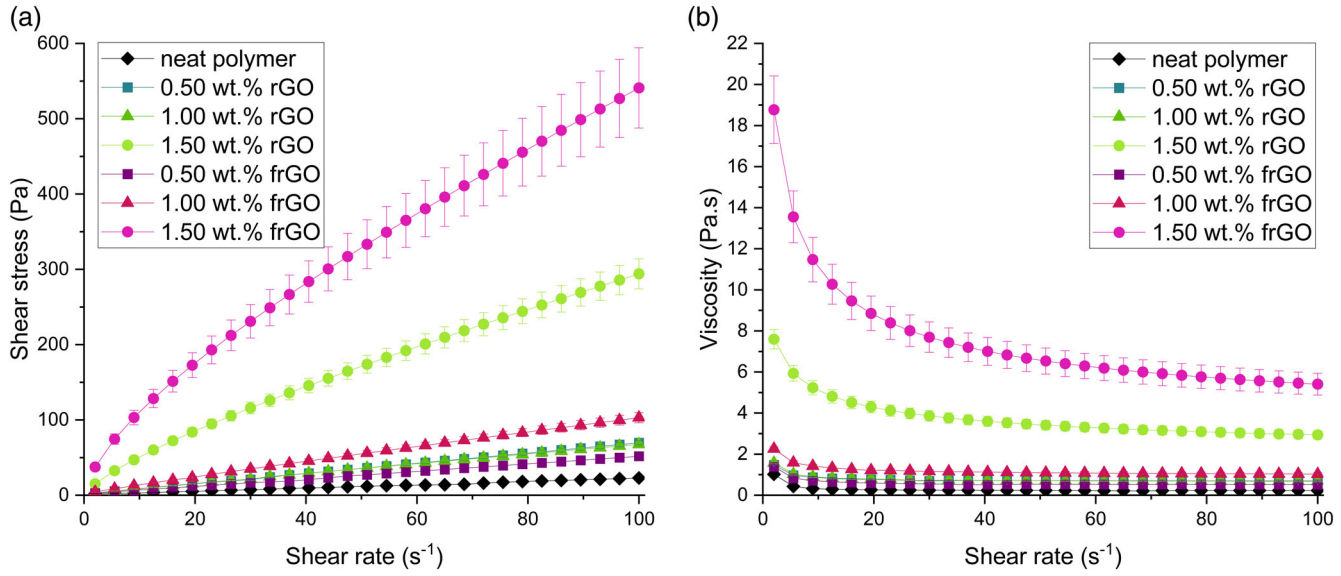

FIGURE 3 Rheological behavior of the examined materials. (a) Mean shear stress versus shear rate of exemplary uncured neat polymer and rGO/frGO-including suspensions with different loadings for the complete range of experienced shear stress (maximum was 541 pa). (b) Mean viscosity versus shear rate of exemplary uncured neat polymer and rGO/frGO-including suspensions with different weight fractions for the complete range of experienced viscosity (maximum was 18.8 Pa s). The error bars (expanded uncertainty) are given for a coverage probability of 95% [Color figure can be viewed at wileyonlinelibrary.com]

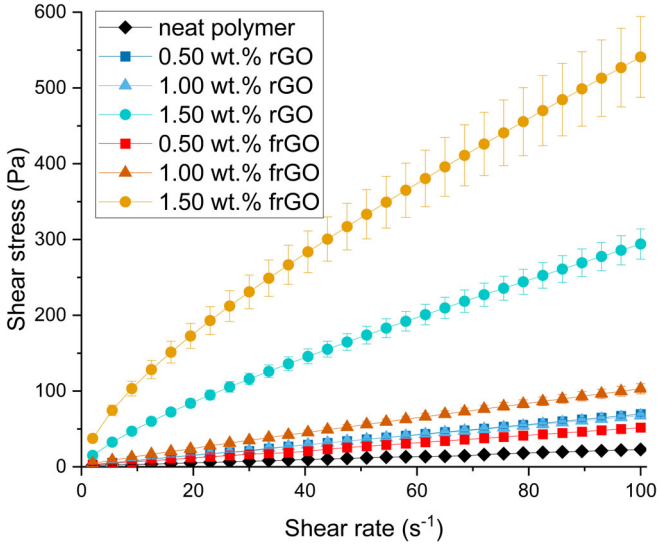

FIGURE 4 Mean shear stress versus weight fractions of uncured neat polymer and rGO/frGO-including suspensions with respect to three exemplary shear rates (2, 51, and 100 s^{-1}). The error bars (expanded uncertainty) are given for a coverage probability of 95% [Color figure can be viewed at wileyonlinelibrary.com]

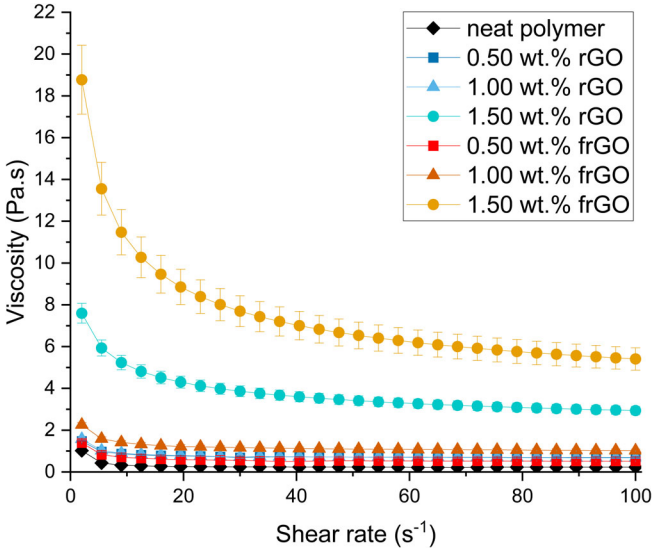

FIGURE 5 Mean viscosity versus weight fractions of uncured neat polymer and rGO/frGO-including suspensions with respect to three exemplary shear rates (2, 51, and 100 s^{-1}). The error bars (expanded uncertainty) are given for a coverage probability of 95% [Color figure can be viewed at wileyonlinelibrary.com]

1.50 wt%. Moreover, a slight drop of the occurring shear stresses was observed for rGO from 0.75 to 1.00 wt% at higher shear rates of 51 and 100 s^{-1} whereas all other samples continued to exhibit increasing shear stresses.

A similar behavior with respect to various particle loadings was observed upon evaluation of the change of viscosity versus shear rate (Figure 3b). With higher weight fractions, an increase of the viscosity was visible for rGO and frGO, but the viscosity of the suspension decreased with increasing shear rates. As such, it can be deduced that both the unfilled polymer as well as the rGO/frGO-containing suspensions exhibited a shear-thinning behavior. Again, the effect of the examined loading was more dominant for nanoparticle contents of 1.00 to 1.50 wt% than for loadings of 0.25 to 1.00 wt%. Upon examination of Figure 5 that shows the change in viscosity with respect to different loadings of rGO and frGO at three exemplary shear rates of 2, 51 and 100 s^{-1}, the same thresholds for a different impact of rGO and frGO were observed as for shear stress versus shear rate: As before, the influence of the additive on the increasing viscosity of the suspension was higher in the case of rGO than for frGO for nanoparticle loadings of 0.25–0.75 wt%. For loadings from 0.75 to 1.50 wt%, the impact on the viscosity was higher for frGO than for rGO. In the case of rGO, a minor drop in the viscosity was present from 0.75 to 1.00 wt% at higher shear rates of 51[1] and 100 s^{-1} whereas the other samples continued to show a viscosity increase.

3.3 | Curing behavior of reduced graphene oxide/epoxy nanocomposites

The reaction enthalpy of a curing reaction can be used to estimate the exothermic behavior and, hence, the ease of process control for composite production. The DSC thermograms of three exemplary samples with different loadings are illustrated in Figure 6 and the analytical results of the DSC test series are listed in Table 3. This implies that the curing reaction was marginally faster in the case of the additive-including suspensions below the exothermic peak temperature than for the neat epoxy, but was slower above the exothermic peak temperature which leads to similar cure durations of all samples. This was also apparent from the conversion rates (Figure 7) that illustrate that higher weight fractions led to a faster conversion until the exothermic peak temperature was reached. The conversion rate α is typically used to describe the reaction kinetics by evaluating the partial integral of the heat flow $\Delta H(T)$ at a temperature T with respect to the total reaction enthalpy of the chemical reaction ΔH_R[53,54]:

$$\alpha(T) = \frac{\Delta H(T)}{\Delta H_R} = \frac{\int_{T_o}^{T} \frac{dH}{dT}\, dT}{\int_{T_o}^{T_e} \frac{dH}{dT}\, dT}, \quad (1)$$

where T_o is the onset temperature and T_e is the end temperature of curing. The thermograms of the epoxy/reduced graphene oxide suspensions are slightly shifted

to the left whilst showing similar onset and end temperatures of curing. After the exothermic peak temperature, the gradient of the conversion rates decreased. This decrease after the exothermic peak temperature was more prominent with increasing particle loadings. The overall effect of the used additives on the conversion rates was higher in the case of rGO than for frGO. The reaction enthalpy of the curing reaction was affected by the presence of the used graphene derivatives. There was, however, only a significant increase of the reaction enthalpy

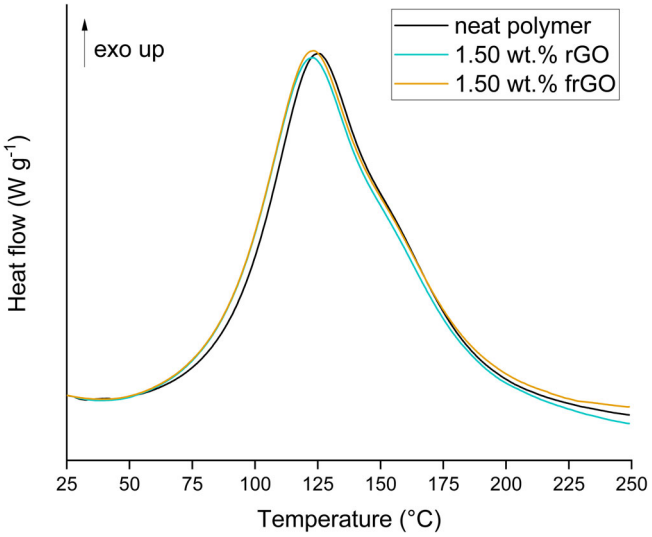

FIGURE 6 Differential scanning calorimetry thermograms of the curing reaction of the uncured neat polymer and two exemplary additive-including suspensions (1.50 wt% rGO and 1.50 wt% frGO) [Color figure can be viewed at wileyonlinelibrary.com]

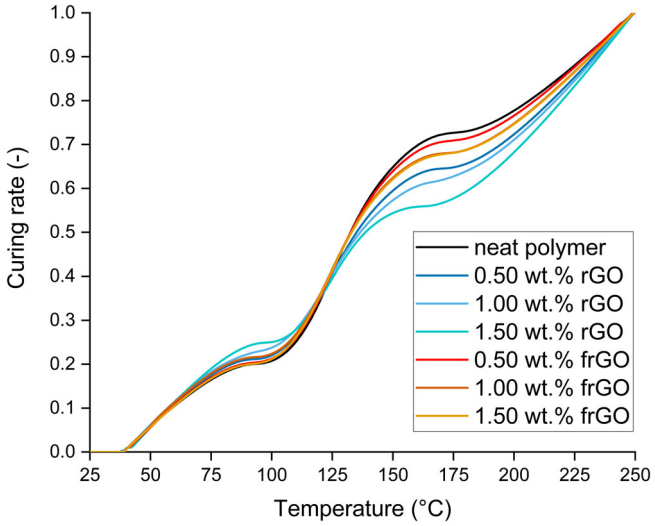

FIGURE 7 Exemplary mean conversion rates of the curing reactions of uncured neat polymer and additive-including suspensions as determined from differential scanning calorimetry [Color figure can be viewed at wileyonlinelibrary.com]

TABLE 3 Characteristic parameters of the conducted differential scanning calorimetry experiments with respective expanded uncertainty for a coverage probability of 95%

Material	T_o (°C)[a]	T_p (°C)[b]	T_e (°C)[c]	Cure range (°C)[d]	Cure duration (min)[e]	ΔH_R (J g^{-1})[f]
Neat polymer	38 ± 1	126 ± 0	248 ± 0	210 ± 0	21.0 ± 0.0	480 ± 21
0.25 wt% rGO	39 ± 2	125 ± 0	248 ± 0	209 ± 2	20.9 ± 0.2	515 ± 8
0.50 wt% rGO	39 ± 2	124 ± 1	248 ± 0	209 ± 2	20.9 ± 0.2	490 ± 20
0.75 wt% rGO	38 ± 1	124 ± 1	248 ± 0	209 ± 2	20.9 ± 0.2	522 ± 25
1.00 wt% rGO	38 ± 1	123 ± 1	248 ± 0	210 ± 1	21.0 ± 0.1	473 ± 21
1.25 wt% rGO	38 ± 0	124 ± 0	247 ± 0	210 ± 0	21.0 ± 0.0	511 ± 10
1.50 wt% rGO	39 ± 1	123 ± 0	248 ± 0	209 ± 1	20.9 ± 0.1	533 ± 7
0.25 wt% frGO	37 ± 0	124 ± 0	248 ± 0	210 ± 1	21.0 ± 0.1	511 ± 25
0.50 wt% frGO	38 ± 1	125 ± 2	247 ± 2	209 ± 3	20.9 ± 0.3	505 ± 13
0.75 wt% frGO	37 ± 0	125 ± 0	248 ± 0	210 ± 0	21.0 ± 0.0	518 ± 9
1.00 wt% frGO	37 ± 0	124 ± 0	247 ± 0	210 ± 0	21.0 ± 0.0	496 ± 6
1.25 wt% frGO	37 ± 1	123 ± 1	248 ± 0	211 ± 1	21.1 ± 0.1	485 ± 20
1.50 wt% frGO	37 ± 0	123 ± 0	248 ± 0	210 ± 0	21.0 ± 0.0	482 ± 19

[a]Onset temperature of curing.
[b]Exothermic peak temperature.
[c]End temperature of curing.
[d]Total temperature range of curing reaction, equal to the temperature difference of T_o and T_e.
[e]Elapsed time of curing reaction based on the time difference at which T_o and T_e occur.
[f]Specific reaction enthalpy of curing reaction.

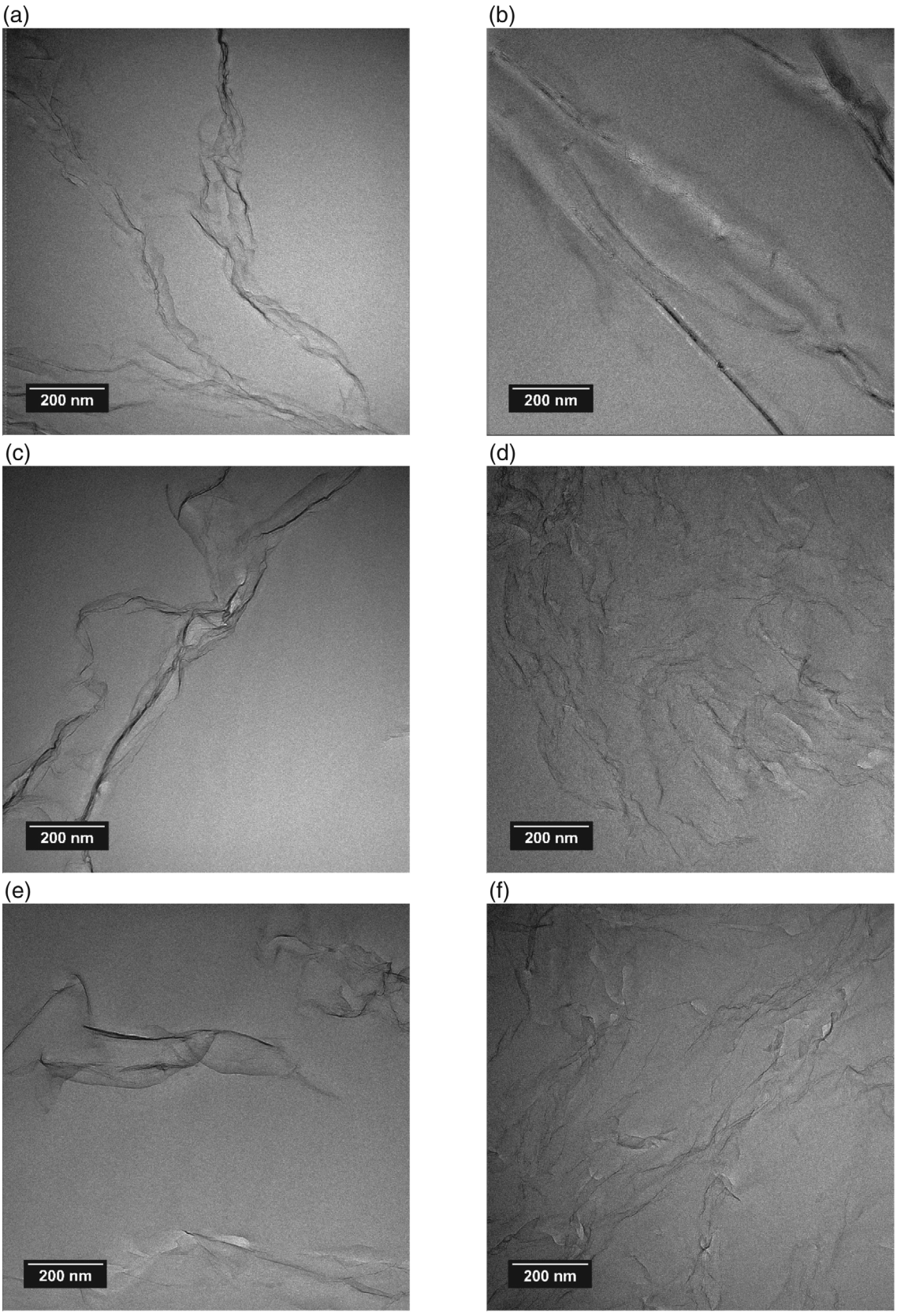

FIGURE 8 Transmission electron microscopy images of rGO and frGO nanocomposite samples taken at a magnification of 40,000×. (a) 0.50 wt% rGO, (b) 0.50 wt% frGO, (c) 1.00 wt% rGO, (d) 1.00 wt% frGO, (e) 1.50 wt% rGO and (f) 1.50 wt% frGO

for the sample that included 1.50 wt% rGO. As an amine-based hardener is used in conjunction with an amine-functionalization of the particles, one might expect that the reaction enthalpy would be increased in the case of frGO. Given that this effect cannot be observed in the DSC data, it can be assumed that partial curing took place while the frGO particles were dispersed in the epoxy resin without the addition of the hardener in the three roll mill.

3.4 | Homogeneity of dispersion of the reduced graphene oxide particles in the nanocomposite matrix

A homogeneous distribution of the graphene-related additive in the matrix is crucial to achieve a consistent quality of the material. TEM images taken of representative areas of the rGO and frGO nanocomposite samples (Figure 8) were used to evaluate the interface of the graphene-related particles with the matrix and hereby the degree of dispersion. The rGO inclusions in the nanocomposite samples remained clearly visible with areas of strong contrast at all loadings indicating a small degree of agglomeration. In contrast to this, the frGO inclusions appeared more obscure suggesting a good dispersion of the functionalized material in the matrix. However, it should be pointed out that all samples demonstrated improved dispersion of the particles with increasing weight fractions of the used additives. This can be attributed to the higher viscosity of the suspensions hindering the particles from forming agglomerates during processing and curing at high loadings.

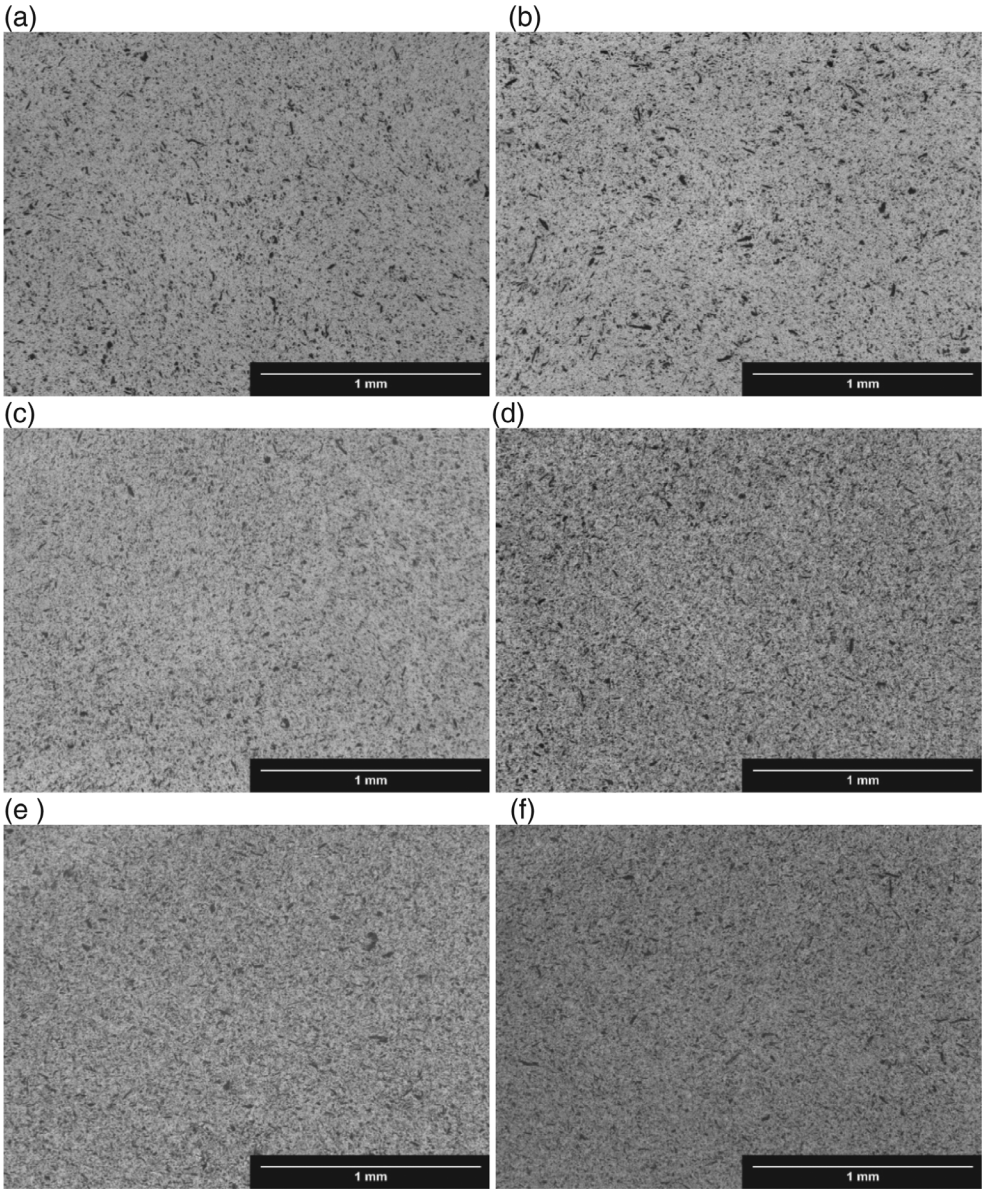

FIGURE 9 Thin sections of rGO and frGO nanocomposite samples taken at a magnification of 63×. (1) 0.50 wt% rGO, (2) 0.50 wt% frGO, (3) 1.00 wt% rGO, (4) 1.00 wt% frGO, (5) 1.50 wt.% rGO and (6) 1.50 wt% frGO

By evaluating thin sections of the nanocomposite materials with an optical microscope, it is possible to examine the broad degree of dispersion within the specimen as well as potential flotation or sedimentation. The thin sections of exemplary nanocomposite samples are shown in Figure 9. All samples displayed no flotation or sedimentation implying a homogeneous distribution of the particles along the height of the specimen. Similar to the TEM analysis, the frGO nanocomposite samples showed fewer agglomerates at higher weight fractions as indicated by the darker appearance of these samples. In contrast to this, the rGO nanocomposite exhibited more particle-rich (dark) and resin-rich areas as suggested by the brighter appearance of the samples through which light can pass through more easily.

4 | SUMMARY

In this work, the influence of an amine-functionalization of reduced graphene oxide particles on the viscosity and the curing reaction of an epoxy system was investigated. A characterization of the quality of the rGO and frGO powders by Raman spectroscopy and BET analysis showed that the plasma functionalization process of the used additives has a significant effect on the number of defects and no significant effect on the specific surface area of the particles. The processing behavior of the suspensions for composite manufacturing was estimated from the rheological and curing behavior. The viscosity change due to the addition of the used graphene derivatives was determined by the use of a rheometer. A shear-thinning behavior was observed for all samples. Furthermore, it can be concluded that increasing weight fractions lead to an increasing viscosity of the suspensions. This effect was more severe if a threshold of a loading of 1.00 wt% was exceeded and more significant in the case of frGO than for rGO. Taking a shear rate of 2 s^{-1} as an example, the presence of 1.00 wt% frGO (rGO) led to a 2-fold (2-fold) increase of the viscosity whereas the incorporation of 1.50 wt% frGO (rGO) led to a 18-fold (7-fold) increase of the viscosity. The curing behavior of the suspensions was analyzed by the use of differential scanning calorimetry. The reaction enthalpy of the curing reaction is affected by the addition of the graphene-related material to the matrix, but there is only a significant increase at 1.50 wt% rGO. Furthermore, the presence of the used particles influences the conversion rate of the curing reaction. Higher weight fractions lead to an increase in the conversion rate until the exothermic peak temperature is reached. After the exothermic peak temperature, the conversion rates of the suspensions with particulate inclusions are lower than the conversion rate of the neat polymer. This effect is more dominant in the case of rGO than for frGO which might be deduced from the partial curing of the amine-functionalized particles during the dispersion process. The cure range and cure duration are not significantly affected by the presence of the used additives. As shown by TEM and optical microscopy of thin sections, the tailored functionalization of the frGO particles helped to improve the homogeneity of dispersion of the particles in the epoxy matrix especially at higher weight fractions. At reduced weight fractions, the low viscosity of the suspension resulted in a more facile formation of agglomerates.

ACKNOWLEDGMENTS

This research and development project is funded by the German Federal Ministry of Education and Research (BMBF) within the framework concept "Forschungscampus" ARENA2036 (funding number: 02P18Q643) and managed by the Project Management Agency Karlsruhe (PTKA). The author is responsible for the contents of this publication. Additionally, the TEM was funded by the German Research Foundation (DFG Inst275/391-1). The authors also thank Graphit Kropfmühl GmbH and Sika Deutschland GmbH for the supply of materials, Hans-Jürgen Hempel (Friedrich-Schiller-University Jena, Otto Schott Institute of Materials Research) for the preparation of the TEM images, Dr Mhamed Assebban (Friedrich-Alexander University Erlangen-Nürnberg, Institute of Advanced Materials and Processes – ZMP) for the preparation of the Raman measurements and Drs Lachlan Hyde and Nishar Hameed from Swinburne University of Technology for helpful discussions. Open Access funding enabled and organized by Projekt DEAL.

CONFLICT OF INTEREST

The authors declare no conflict of interest.

ORCID

Annika C. Ackermann https://orcid.org/0000-0003-1699-8672

REFERENCES

[1] A. A. Balandin, S. Ghosh, W. Bao, I. Calizo, D. Teweldebrhan, F. Miao, C. N. Lau, *Nano Lett.* **2008**, *8*, 902. https://doi.org/10.1021/nl0731872

[2] K. I. Bolotin, K. J. Sikes, J. Hone, H. L. Stormer, P. Kim, *Phys. Rev. Lett.* **2008**, *101*, 1. https://doi.org/10.1103/PhysRevLett.101.096802

[3] C. Lee, X. Wei, J. W. Kysar, J. Hone, *Science* **2008**, *321*, 385. https://doi.org/10.1126/science.1157996

[4] Y. Zhu, S. Murali, W. Cai, X. Li, J. W. Suk, J. R. Potts, R. S. Ruoff, *Adv. Mater.* **2010**, *22*, 3906. https://doi.org/10.1002/adma.201001068

[5] A. Saritha, S. K. Malhotra, S. Thomas, K. Joseph, K. Goda, M. S. Sreekala, in *Polymer Composites*, Vol. 2 (Eds: S. Thomas, K. Joseph, S. K. Malhotra, K. Goda, M. S. Sreekala), Wiley-VCH, Weinheim, Germany **2013**.

[6] S. Chatterjee, F. Nafezarefi, N. H. Tai, L. Schlagenhauf, F. A. Nüesch, B. T. T. Chu, *Carbon* **2012**, *50*, 5380. https://doi.org/10.1016/j.carbon.2012.07.021

[7] D. G. Papageorgiou, I. A. Kinloch, R. J. Young, *Prog. Mater. Sci.* **2017**, *90*, 75. https://doi.org/10.1016/j.pmatsci.2017.07.004

[8] C. E. Corcione, F. Freuli, A. Maffezzoli, *Polym. Eng. Sci.* **2013**, *53*, 531. https://doi.org/10.1002/pen.23292

[9] Y. T. Park, Y. Qian, C. Chan, T. Suh, M. G. Nejhad, C. W. Macosko, A. Stein, *Adv. Funct. Mater.* **2015**, *25*, 575. https://doi.org/10.1002/adfm.201402553

[10] X. Du, H. Zhou, W. Sun, H.-Y. Liu, G. Zhou, H. Zhou, Y.-W. Mai, *Compos. Sci. Technol.* **2017**, *140*, 123. https://doi.org/10.1016/j.compscitech.2016.12.028

[11] N. T. Kamar, M. M. Hossain, A. Khomenko, M. Haq, L. T. Drzal, A. Loos, *Compos. A* **2015**, *70*, 82. https://doi.org/10.1016/j.compositesa.2014.12.010

[12] A. Pegoretti, H. Mahmood, D. Pedrazzoli, K. Kalaitzidou, *IOP Conf. Ser.: Mater. Sci. Eng.* **2016**, *139*, 1. https://doi.org/10.1088/1757-899X/139/1/012004

[13] W. Qin, F. Vautard, L. T. Drzal, J. Yu, *Compos. B* **2015**, *69*, 335. https://doi.org/10.1016/j.compositesb.2014.10.014

[14] K. Lau, M. Lu, H. Cheung, F. Sheng, H. Li, *Compos. Sci. Technol.* **2005**, *65*, 719. https://doi.org/10.1016/j.compscitech.2004.10.005

[15] M. R. Loos, L. A. F. Coelho, S. H. Pezzin, S. C. Amico, *Polímeros* **2008**, *18*, 76. https://doi.org/10.1590/S0104-14282008000100015

[16] R. J. Zaldivar, P. M. Adams, H. I. Kim, J. P. Nokes, D. N. Patel, *J. Appl. Polym. Sci.* **2014**, *131*, 40802. https://doi.org/10.1002/app.40802

[17] B. Ahmadi-Moghadam, M. Sharafimasooleh, S. Shadlou, F. Taheri, *Mater. Des.* **2015**, *66*, 142. https://doi.org/10.1016/j.matdes.2014.10.047

[18] L.-J. Cui, Y.-B. Wang, W.-J. Xiu, W.-Y. Wang, L.-H. Xu, X.-B. Xu, Y. Meng, L.-Y. Li, J. Gao, L.-T. Chen, H.-Z. Geng, *Mater. Des.* **2013**, *49*, 279. https://doi.org/10.1016/j.matdes.2013.01.050

[19] L. Ma, G. Wang, J. Dai, *J. Appl. Polym. Sci.* **2016**, *133*, 638. https://doi.org/10.1002/app.43820

[20] M. Naderi, F. Ebrahimi, M. Najafi, H. Naderi, *J. Appl. Polym. Sci.* **2019**, *136*, 47475. https://doi.org/10.1002/app.47475

[21] J. A. Kim, D. G. Seong, T. J. Kang, J. R. Youn, *Carbon* **2006**, *44*, 1898. https://doi.org/10.1016/j.carbon.2006.02.026

[22] C. Monteserín, M. Blanco, E. Aranzabe, A. Aranzabe, J. L. Vilas, *J. Appl. Polym. Sci.* **2017**, *134*, 44803. https://doi.org/10.1002/app.44803

[23] M. Seong, D. S. Kim, *J. Appl. Polym. Sci.* **2015**, *132*, 42269. https://doi.org/10.1002/app.42269

[24] A. Alam, C. Wan, T. McNally, *Eur. Polym. J.* **2017**, *87*, 422. https://doi.org/10.1016/j.eurpolymj.2016.10.004

[25] H. Zhang, H. X. Li, H. M. Cheng, *J. Phys. Chem. B* **2006**, *110*, 9095. https://doi.org/10.1021/jp060193y

[26] S. Song, C. Wan, Y. Zhang, *RSC Adv.* **2015**, *5*, 79947. https://doi.org/10.1039/C5RA14967C

[27] A. Hirsch, J. M. Englert, F. Hauke, *Acc. Chem. Res.* **2013**, *46*, 87. https://doi.org/10.1021/ar300116q

[28] J. Park, M. Yan, *Acc. Chem. Res.* **2013**, *46*, 181. https://doi.org/10.1021/ar300172h

[29] I. Bertóti, M. Mohai, K. László, *Carbon* **2015**, *84*, 185. https://doi.org/10.1016/j.carbon.2014.11.056

[30] N. Inagaki, *Plasma Surface Modification and Plasma Polymerization*, Technomic Publishing, Lancaster, UK **1996**.

[31] D. Hegemann, H. Brunner, C. Oehr, *Nucl. Instrum. Methods. Phys. Res. Sect. B* **2003**, *208*, 281. https://doi.org/10.1016/S0168-583X(03)00644-X

[32] J. Paredes, A. Martínez-Alonso, J. M. D. Tascón, *J. Colloid. Interface. Sci.* **2003**, *258*, 276. https://doi.org/10.1016/S0021-9797(02)00146-7

[33] L. Liu, D. Xie, M. Wu, X. Yang, Z. Xu, W. Wang, X. Bai, E. Wang, *Carbon* **2012**, *50*, 3039. https://doi.org/10.1016/j.carbon.2012.02.090

[34] Y. Wang, Z. Iqbal, S. V. Malhotra, *Chem. Phys. Lett.* **2005**, *402*, 96. https://doi.org/10.1016/j.cplett.2004.11.099

[35] A. Maio, L. Botta, A. C. Tito, L. Pellegrino, M. Daghetta, R. Scaffaro, *Plasma Process. Polymer* **2014**, *11*, 664. https://doi.org/10.1002/ppap.201400008

[36] X. Shen, Z. Wang, Y. Wu, X. Liu, J.-K. Kim, *Carbon* **2016**, *108*, 412. https://doi.org/10.1016/j.carbon.2016.07.042

[37] R. Raccichini, A. Varzi, S. Passerini, B. Scrosati, *Nat. Mater.* **2015**, *14*, 271. https://doi.org/10.1038/nmat4170

[38] M. Naebe, J. Wang, A. Amini, H. Khayyam, N. Hameed, L. H. Li, Y. Chen, B. Fox, *Sci. Rrep.* **2014**, *4*, 4375. https://doi.org/10.1038/srep04375

[39] A. J. Marsden, D. G. Papageorgiou, C. Vallés, A. Liscio, V. Palermo, M. A. Bissett, R. J. Young, I. A. Kinloch, *2D Mater.* **2018**, *5*, 32003. https://doi.org/10.1088/2053-1583/aac055

[40] S. Chandrasekaran, C. Seidel, K. Schulte, *Eur. Polym. J.* **2013**, *49*, 3878. https://doi.org/10.1016/j.eurpolymj.2013.10.008

[41] S. Ganguli, A. K. Roy, D. P. Anderson, *Carbon* **2008**, *46*, 806. https://doi.org/10.1016/j.carbon.2008.02.008

[42] A. A. Silva, R. Stein, D. Campos, T. Indrusiak, B. G. Soares, G. M. O. Barra, *Front. Mater.* **2019**, *6*. https://doi.org/10.3389/fmats.2019.00156

[43] M. Reghat, A. Mirabedini, A. M. Tan, Y. Weizman, P. Middendorf, R. Bjekovic, L. Hyde, D. Antiohos, N. Hameed, F. K. Fuss, B. Fox, *Compos. Sci. Technol.* **2021**, *211*, 108842. https://doi.org/10.1016/j.compscitech.2021.108842

[44] J. M. Englert, P. Vecera, K. C. Knirsch, R. A. Schäfer, F. Hauke, A. Hirsch, *ACS Nano* **2013**, *7*, 5472. https://doi.org/10.1021/nn401481h

[45] DIN Deutsches Institut für Normung e.V, *Determination of the Specific Surface Area of Solids by Gas Adsorption - BET Method (ISO 9277:2010)*, Beuth Verlag, Berlin, Germany **2014**.

[46] DIN Deutsches Institut für Normung e.V, *Aerospace - Testing of Thermosetting Resin Systems with and without Reinforcement - DSC Method*, Beuth Verlag, Berlin, Germany **1999**.

[47] A. C. Ferrari, J. Robertson, *Phys. Rev. B* **2000**, *61*, 14095. https://doi.org/10.1103/PhysRevB.61.14095

[48] A. C. Ferrari, D. M. Basko, *Nat. Nanotechnol.* **2013**, *8*, 235. https://doi.org/10.1038/nnano.2013.46

[49] M. D. Stoller, S. Park, Y. Zhu, J. An, R. S. Ruoff, *Nano Lett.* **2008**, *8*, 3498. https://doi.org/10.1021/nl802558y

[50] Z. Fan, K. Wang, T. Wei, J. Yan, L. Song, B. Shao, *Carbon* **2010**, *48*, 1686. https://doi.org/10.1016/j.carbon.2009.12.063

[51] Y. Wang, Z. Shi, Y. Huang, Y. Ma, C. Wang, M. Chen, Y. Chen, *J. Phys. Chem. C* **2009**, *113*, 13103. https://doi.org/10.1021/jp902214f

[52] V. B. Mohan, K. Jayaraman, D. Bhattacharyya, *Solid State Commun.* **2020**, *320*, 114004. https://doi.org/10.1016/j.ssc.2020.114004
[53] M. Wagner, *Thermal Analysis in Practice: Fundamental Aspects*, Carl Hanser Verlag, Munich, Germany **2018**.
[54] S. Park, D. S. Kim, *Polym. Eng. Sci.* **2014**, *54*, 985. https://doi.org/10.1002/pen.23368

How to cite this article: A. C. Ackermann, S. Carosella, M. Rettenmayr, B. L. Fox, P. Middendorf, *J. Appl. Polym. Sci.* **2022**, *139*(8), e51664. https://doi.org/10.1002/app.51664